

ADA 081 436

Communications Research Centre

3

LEVEL

DTIC
SELECTED
FEB 28 1980
C

AN ANALYSIS OF THE BACK-SCATTERING PROPERTIES OF A CLUSTER OF CORNER REFLECTORS AT X-BAND FREQUENCIES

by
B.J. Rook

This work was sponsored by the Department of National Defence, Research and Development Branch,
under Project No. 33C61.

DEPARTMENT OF COMMUNICATIONS
MINISTÈRE DES COMMUNICATIONS

CRC REPORT NO. 1328

FILE COPY

CANADA

OTTAWA, OCTOBER 1979

80 2 26 029

COMMUNICATIONS RESEARCH CENTRE

DEPARTMENT OF COMMUNICATIONS
CANADA

3
S DTIC ELECTE D
FEB 28 1980

C

6

AN ANALYSIS OF THE BACK-SCATTERING PROPERTIES OF A CLUSTER OF CORNER REFLECTORS AT X-BAND FREQUENCIES

by

B.J. Rook

(Radio and Radar Research Branch)

14

CRC REPORT NO. 132B

120
25

11

October 1979

OTTAWA

This work was sponsored by the Department of National Defence, Research and Development Branch, under Project No. 33C61.

CAUTION

The use of this information is permitted subject to recognition of proprietary and patent rights.

402 107

YB

TABLE OF CONTENTS

ABSTRACT 1

1. INTRODUCTION 1

2. EXPRESSION FOR THE RADAR CROSS-SECTION 3

3. DETERMINATION OF THE EFFECTIVE BACK-SCATTERING AREA 5

 3.1 Effective Back-Scattering Area Due to One Reflection 5

 3.1.1 Effective Back-Scattering Area Due to One Reflection From
 Cluster Surfaces 7

 3.2 Effective Back-Scattering Area Due to Two Reflections 9

 3.2.1 Effective Back-Scattering Area Due to Two Reflections From
 Cluster Surfaces 10

 3.3 Effective Back-Scattering Area Due to Three Reflections 12

 3.3.1 Effective Back-Scattering Area Due to Three Reflections
 From Cluster Surfaces 12

4. DETERMINATION OF THE RADAR CROSS-SECTION FOR A CLUSTER OF CORNER
REFLECTORS 13

5. DISCUSSION OF RESULTS FOR A CLUSTER OF FOUR SQUARE-CORNER REFLECTORS . 14

 5.1 Discussion of Results of the Average Radar Cross-section for a
 Cluster of Four Square-Corner Reflectors 18

6. CALCULATION OF THE AVERAGE RADAR CROSS-SECTION FOR THE CLUSTER
ILLUSTRATED IN FIGURE 1 18

7. SUMMARY AND CONCLUSIONS 22

8. ACKNOWLEDGEMENTS 22

9. REFERENCES 22

Accession For	
NTIS GMA&I	<input checked="" type="checkbox"/>
DDC TAB	<input type="checkbox"/>
Unannounced Justification	<input type="checkbox"/>
By _____	
Distribution/ Availability Codes	
Dist	Avail and/or special
A	

AN ANALYSIS OF THE BACK-SCATTERING PROPERTIES OF A CLUSTER OF CORNER
REFLECTORS AT X-BAND FREQUENCIES

by

B. J. Rook

ABSTRACT

A study of the back-scattering properties of a cluster of four square-corner reflectors is carried out, and the results used to calculate approximately the radar cross-section of a cluster of four corner reflectors with a circular back-plate. It is shown that this cluster of corner reflectors with sides 0.225 metres long has an average radar cross-section greater than one square-metre over a wide range of incident angles at X-Band frequencies.

1. INTRODUCTION

In response to a requirement of the Defence Research Establishment Suffield (DRES), Alberta, a study has been made of the back-scattering properties of a cluster of four corner reflectors of the type illustrated in Figure 1, at X-Band frequencies. This cluster, which has a circular back-plate, is housed in a sleeve attached to a miss-distance indicator. The complete assembly is towed behind an aircraft and tracked by a radar to provide tracking information for a ground-based gunnery system.

The simplicity of the configuration makes an analytical solution feasible. The radar cross-section of a cluster of four square-corner reflectors of the type illustrated in Figure 2 is calculated, and an approximation is used to allow for the effect of the circular back-plate.

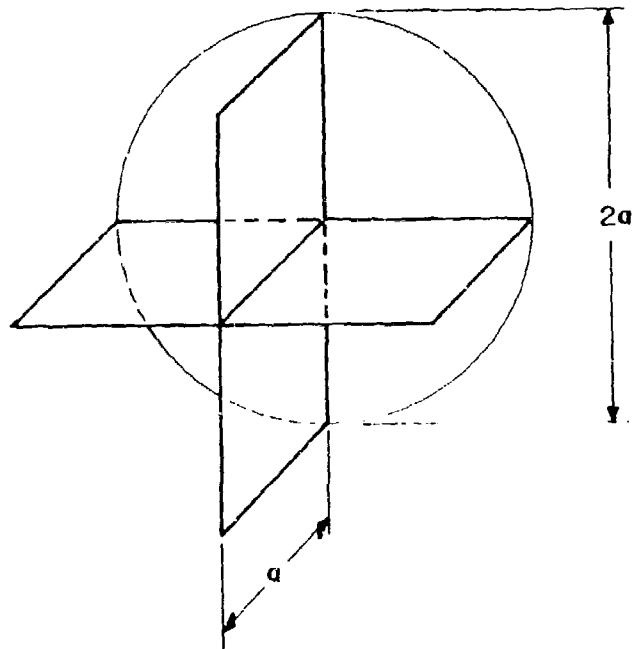


Figure 1. Diagram of a cluster of corner reflectors with a circular back-plate

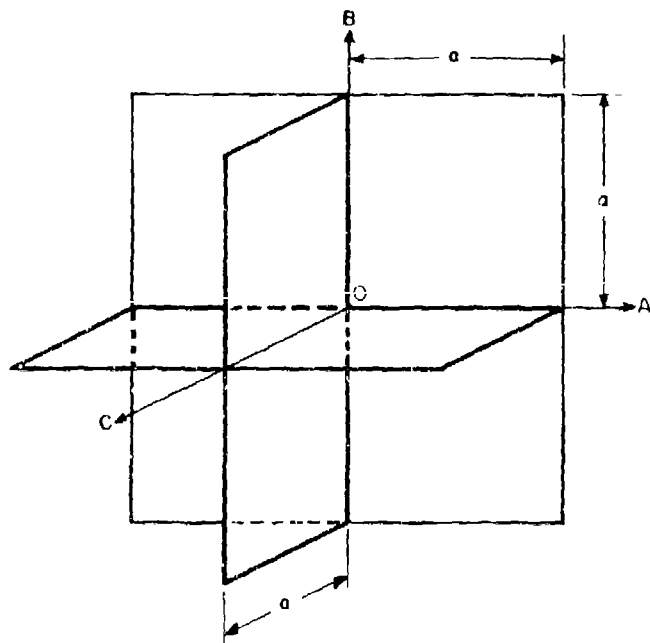


Figure 2. Diagram of a cluster of four square-corner reflectors

A square-corner reflector, which is illustrated in Figure 3, is one of a familiar class of targets designed to maintain a high radar-echoing efficiency over a wide range of incident angles. Extensive analytical work on the back-scattering properties of these targets was carried out by Spencer^[1] in 1944 and later by Robertson^[2] in 1947. This reflector back-scatters incident energy by (a) a triple-reflection process from the three mutually perpendicular sides, (b) a double reflection process from two of the corner surfaces and (c) a single reflection process from one of the corner surfaces. The intensity of this back-scattered radiation may be represented by an equivalent effective back-scattering area which is dependent on the orientation of the source of the radiation relative to the reflector. Thus, the corner reflector behaves as though it were a flat reflecting surface normal to the incident energy and re-radiating energy in the direction whence it came.

In Section 2 of this report, an expression for the radar cross-section is derived in terms of the effective back-scattering area. The determination of the effective back-scattering area and radar cross-section for the cluster in Figure 2 is presented in Sections 3 and 4. Results are presented in Section 5 to illustrate the back-scattering properties of a cluster of four square-corner reflectors at X-Band frequencies. The results from Section 5 are then used to calculate approximate values of the average radar cross-section of the cluster in Figure 1.

2. EXPRESSION FOR THE RADAR CROSS-SECTION

The corner reflector is a passive device for enhancing the back-scattering of electromagnetic radiation. It is important to know the directivity gain, power gain and hence the radar cross-section of such devices if they are to be used as targets for determining the performance of radar systems.

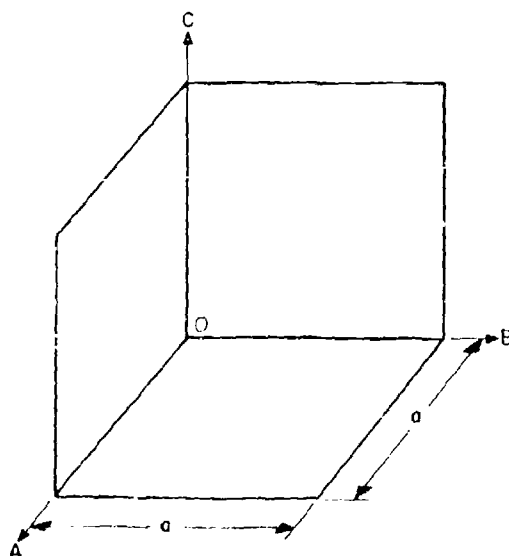


Figure 3. Diagram of a square-corner reflector

With respect to the coordinate system in Figure 4, the power gain $G(\theta, \phi)$ and the directivity gain $D(\theta, \phi)$ are related by^[3]

$$G(\theta, \phi) = \eta D(\theta, \phi) \quad (1)$$

where

θ = azimuth angle

ϕ = elevation angle

η = efficiency parameter.

The efficiency parameter, η , takes into account the reduction in power delivered to the radiator due to ohmic and mismatch losses. In this report, η is assumed to be unity and therefore $G(\theta, \phi) = D(\theta, \phi)$. This assumes that the corner reflector has no power losses, that is, it has zero surface absorption. The power gain may be defined as the ratio of the maximum radiation intensity (power density) from the subject radiator to the radiation intensity of a lossless isotropic radiator with the same power input. Since the corner reflector behaves like a flat reflecting surface normal to the direction of the incident energy, its power gain $G(\theta, \phi)$ relative to a lossless isotropic radiator is the power gain of a uniformly illuminated aperture^[4] given by

$$G(\theta, \phi) = \frac{4\pi A_e(\theta, \phi)}{\lambda^2} \quad (2)$$

where $A_e(\theta, \phi)$ is the effective back-scattering area of the aperture and λ is the free-space wavelength. The radar cross-section $\sigma(\theta, \phi)$ may be determined from equation (2) giving

$$\sigma(\theta, \phi) = GA_e(\theta, \phi) = \frac{4\pi[A_e(\theta, \phi)]^2}{\lambda^2} \quad (3)$$

The parameter $\sigma(\theta, \phi)$ may be used in the *radar equation*^[5] together with the given set of radar system parameters in order to calculate the performance to be expected of the radar as a detection or measurement device. Therefore, such problems involving corner reflectors reduce to the calculation of the effective back-scattering area as a function of the direction of the incident energy.

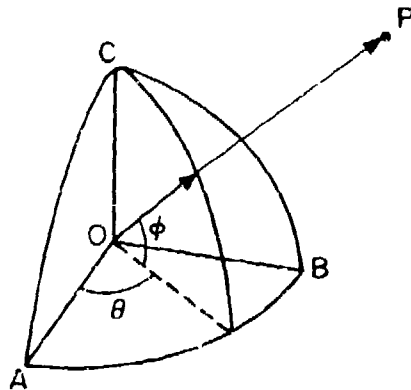


Figure 4. Spherical coordinate system defining θ and ϕ

3. DETERMINATION OF THE EFFECTIVE BACK-SCATTERING AREA

The effective area of a corner reflector due to back-scattering may be written as the sum of three terms,

$$\Lambda_e(\theta, \phi) = \Lambda_e^{(1)}(\theta, \phi) + \Lambda_e^{(2)}(\theta, \phi) + \Lambda_e^{(3)}(\theta, \phi) \quad (4)$$

where

$\Lambda_e^{(1)}(\theta, \phi)$ = effective area due to one reflection only

$\Lambda_e^{(2)}(\theta, \phi)$ = effective area due to two reflections, and

$\Lambda_e^{(3)}(\theta, \phi)$ = effective area due to three reflections.

In the computation of equation (4), the relative phases among $\Lambda_e^{(1)}(\theta, \phi)$, $\Lambda_e^{(2)}(\theta, \phi)$ and $\Lambda_e^{(3)}(\theta, \phi)$ shall be ignored. Therefore, $\Lambda_e(\theta, \phi)$ becomes the average of the effective back-scattering area in the neighbourhood of θ and ϕ . Expressions for $\Lambda_e^{(1)}(\theta, \phi)$, $\Lambda_e^{(2)}(\theta, \phi)$ and $\Lambda_e^{(3)}(\theta, \phi)$ are derived in this section according to the coordinate system given in Figure 4.

3.1 EFFECTIVE BACK-SCATTERING AREA DUE TO ONE REFLECTION

An expression for the effective area due to one reflection from a surface of the corner reflector will be derived. Since this is important only at near normal incidence to the surface under consideration, the presence of the other surfaces may be ignored. Figure 5 illustrates the geometry of the situation. Here, ODEF is a square surface with sides of length a on the OAB plane; P is the position of the radar where radiation is emitted and scattered radiation is measured; Q is a point scatterer on the surface ODEF.

The effective area due to back-scattering from surface ODEF may be written as a double integral

$$\Lambda_e^{(1)}(\theta, \phi) = K \int_{\alpha=0}^a \int_{\beta=0}^a \exp\{j[\omega t - 2|\vec{R} - \vec{r}| \cdot \frac{2\pi}{\lambda}]\} d\alpha d\beta \quad (5)$$

where

K = scale factor to be determined later,

ω = carrier frequency in radians per second,

t = time parameter,

\vec{R} = position vector for point P = $(R\cos\phi \cos\theta, R\cos\phi \sin\theta, R\sin\phi)$, relative to origin O,

\vec{r} = position vector for point Q = $(\alpha, \beta, 0)$, and

$(\alpha, \beta, 0)$ = coordinates of point Q on surface ODEF.

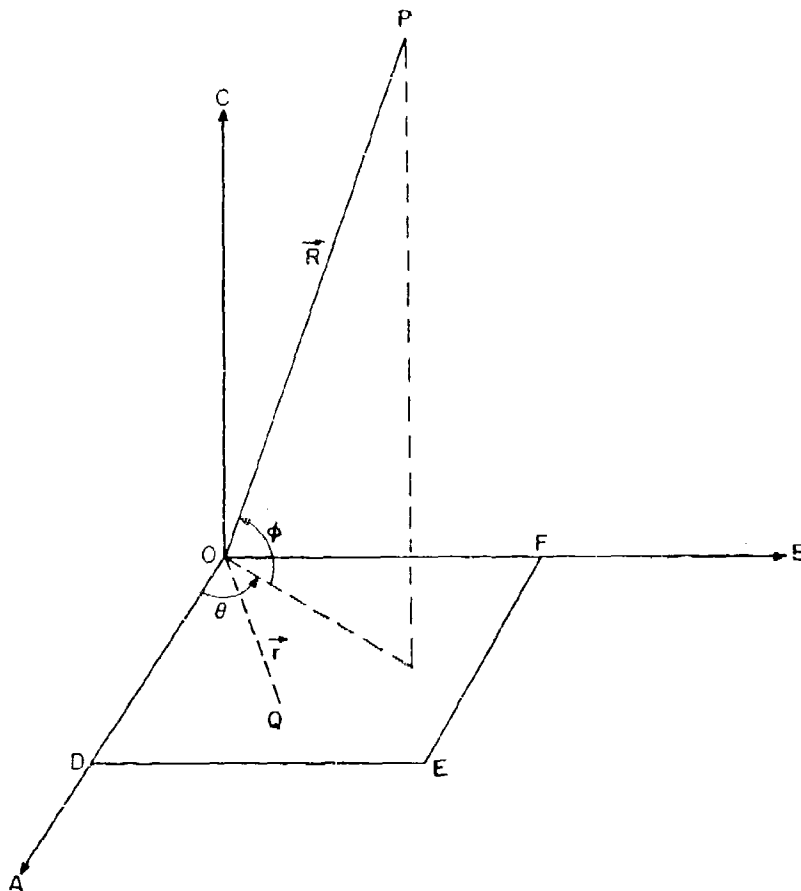


Figure 5. Diagram for calculating the dependence of $A_e^{(1)}(\theta=0, \phi)/a^2$ on ϕ

The term $2|\vec{R} - \vec{r}|$ represents the distance travelled by electromagnetic radiation in its round trip from P to Q and

$$\vec{R} - \vec{r} = (R \cos \phi \cos \theta - \alpha, R \cos \phi \sin \theta - \beta, R \sin \phi). \quad (6)$$

In practice, $|\vec{R}| \gg |\vec{r}|$ and therefore one may write

$$|\vec{R} - \vec{r}| = \{ [R \cos \phi \cos \theta - \alpha]^2 + [R \cos \phi \sin \theta - \beta]^2 + R^2 \sin^2 \phi \}^{1/2} \quad (7)$$

$$\approx [R^2 - 2R(\alpha \cos \phi \cos \theta + \beta \cos \phi \sin \theta)]^{1/2} \quad (8)$$

$$\approx R - (\alpha \cos \phi \cos \theta + \beta \cos \phi \sin \theta). \quad (9)$$

Thus,

$$A_e^{(1)}(\theta, \phi) = K \exp\left\{j\left[\omega t - \frac{4\pi R}{\lambda}\right]\right\} \int_{\alpha=0}^a \int_{\beta=0}^a \exp\{j[4\pi(\alpha \cos\phi \cos\theta + \beta \cos\phi \sin\theta)]\} d\alpha d\beta \quad (10)$$

$$= Ka^2 \exp\left\{j\left[\omega t - \frac{4\pi R}{\lambda} + \frac{2\pi a}{\lambda} \cos\phi \cos\theta + \frac{2\pi a}{\lambda} \cos\phi \sin\theta\right]\right\}$$

$$\cdot \frac{\sin(2\pi a \cos\phi \cos\theta/\lambda)}{2\pi a \cos\phi \cos\theta/\lambda} \cdot \frac{\sin(2\pi a \cos\phi \sin\theta/\lambda)}{2\pi a \cos\phi \sin\theta/\lambda} \quad (11)$$

Since one is only interested in the magnitude of $A_e^{(1)}(\theta, \phi)$, the phase factor on the right hand side of equation (11) may be ignored and the magnitude of the remainder taken. The constant, K , is unity in the case of zero surface absorption because one must have

$$A_e^{(1)}(\theta=0, \phi=90) = a^2, \text{ if } \eta = 1. \quad (12)$$

Hence, in general

$$A_e^{(1)}(\theta, \phi) = a^2 \left| \frac{\sin(2\pi a \cos\phi \cos\theta/\lambda)}{2\pi a \cos\phi \cos\theta/\lambda} \right| \cdot \left| \frac{\sin(2\pi a \cos\phi \sin\theta/\lambda)}{2\pi a \cos\phi \sin\theta/\lambda} \right| \quad (13)$$

A plot of $A_e^{(1)}(\theta=0, \phi)/a^2$ as a function of $2\pi a \cos\phi/\lambda$ is presented in Figure 6.

3.1.1 Effective Back-Scattering Area Due to One Reflection From Cluster Surfaces

Using the solution for one reflection given in equation (13) as a guide, the effective back-scattering area due to one reflection from the cluster surfaces of Figure 2 may be expressed as,

$$A_e^{(1)}(\theta, \phi) = 4a^2 \left| \frac{\sin(4\pi a \cos\phi \cos\theta/\lambda)}{4\pi a \cos\phi \cos\theta/\lambda} \right| \left| \frac{\sin(4\pi a \cos\phi \sin\theta/\lambda)}{4\pi a \cos\phi \sin\theta/\lambda} \right|$$

$$\cdot \frac{[1 + \text{sign}(\sin\phi)]}{2}$$

$$+ 2a^2 \left| \frac{\sin(2\pi a \cos\phi \cos\theta/\lambda)}{2\pi a \cos\phi \cos\theta/\lambda} \right| \left| \frac{\sin(2\pi a \sin\phi)}{2\pi a \sin\phi} \right|$$

$$+ 2a^2 \left| \frac{\sin(2\pi a \sin\phi/\lambda)}{2\pi a \sin\phi/\lambda} \right| \left| \frac{\sin(2\pi a \cos\phi \sin\theta/\lambda)}{2\pi a \cos\phi \sin\theta/\lambda} \right| \quad (14)$$

The first term in equation (14) is the effective back-scattering area from the surface on the OAB plane. It has four times the physical area of

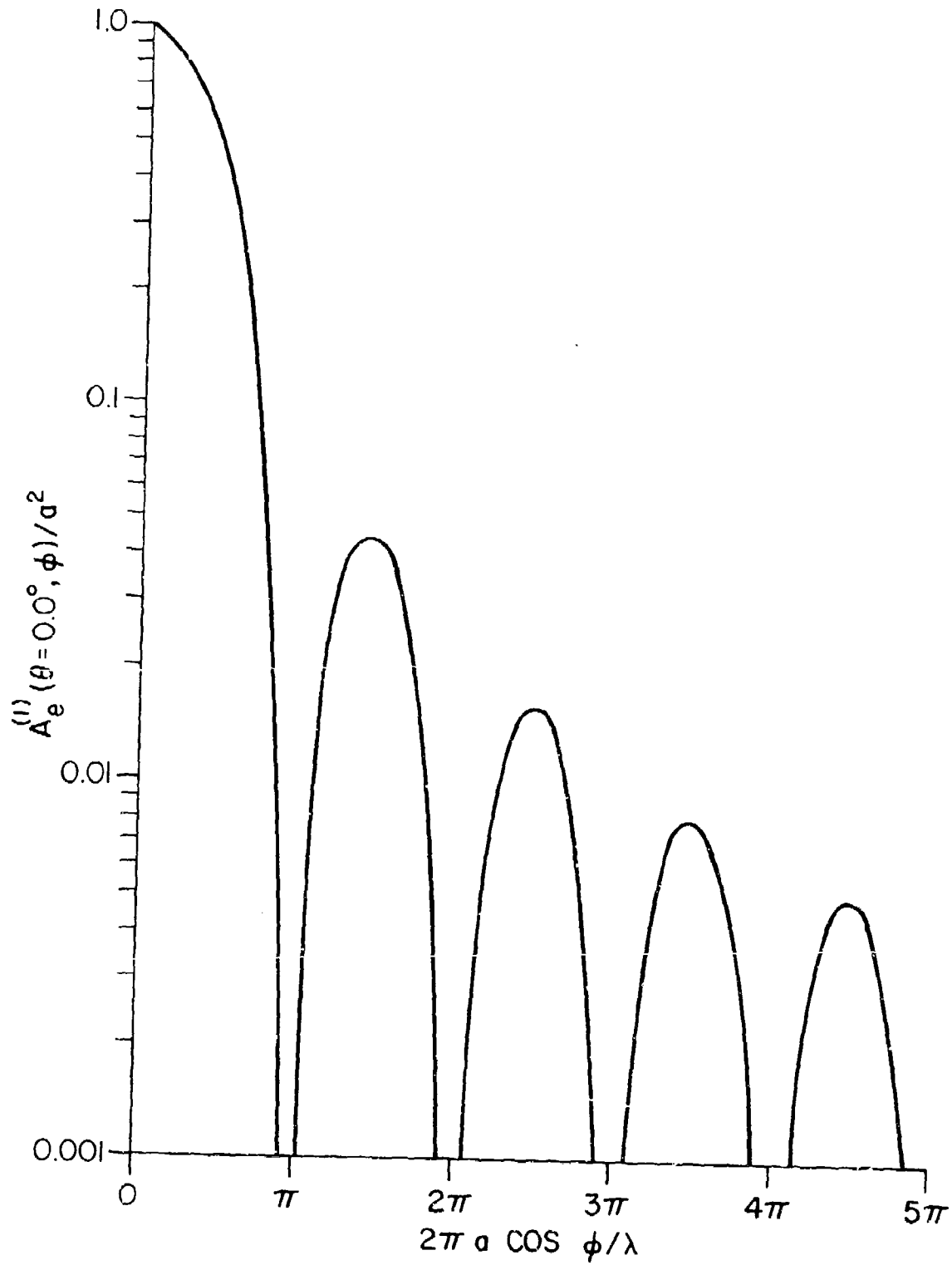


Figure 6. Plot of $A_e^{(1)}(\theta=0, \phi)/a^2$ as a function of $2\pi a \cos \phi/\lambda$

one surface of an individual corner reflector. The second term is the effective back-scattering area from two surfaces on the OAC plane, each having twice the physical area of one surface of an individual corner reflector. The third term, which is similar to the second term, is the effective back-scattering area from two surfaces on the OBC plane. The factor $[1 + \text{sign}(\sin\phi)]/2$ has been included in the first term of equation (14) since we are not interested in back-scattering of electromagnetic energy from the reverse side of the cluster.

3.2 EFFECTIVE BACK-SCATTERING AREA DUE TO TWO REFLECTIONS

The effective back-scattering area due to two reflections from a corner reflector can be calculated in terms of double reflections from diplanes. There are three diplanes in the corner reflector. The seam axes of these diplanes are labelled OA, OB and OC in Figure 7. The definition of the remaining symbols in this figure are as follows:

- P = position of the radar
- \vec{OS} = unit vector along OP
- \vec{OT} = projection of \vec{OS} onto the OBC plane
- ψ = angle between OB and OT
- $(\cos\phi \cos\theta, \cos\phi \sin\theta, \sin\phi)$ = direction cosines of \vec{OS} .

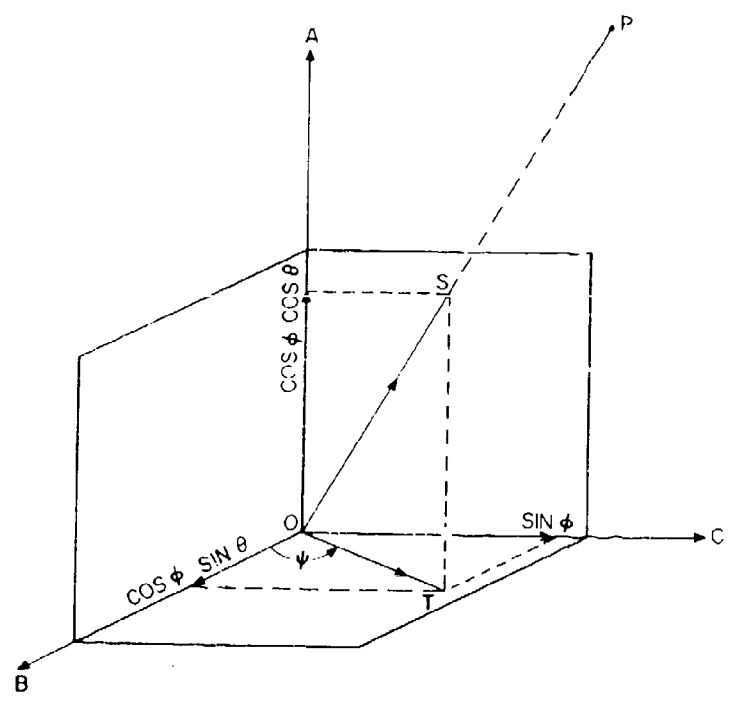


Figure 7. Diagram for calculating the dependence of $A_e^{(2)}(\theta=90,\phi)/a^2$ on ϕ

The effective back-scattering area due to two reflections from the diplane with seam axis OA will be derived here. The effective back-scattering areas due to diplanes with seam axes OB and OC can be determined from the result with seam axis OA by permutation of the direction cosines.

According to the analysis of R.C. Spencer in Reference^[1], effective back-scattering area due to the diplane with seam axis OA may be written as a product of two terms.

$$A_e^{(2)}(\theta, \phi) = \left| \frac{a \sin(2\pi a \cos\phi \cos\theta/\lambda)}{2\pi a \cos\phi \cos\theta/\lambda} \right| \cdot \begin{cases} 2a \sin\psi & , 0^\circ \leq \psi \leq 45^\circ \\ 2a \sin(90-\psi) & , 45^\circ < \psi \leq 90^\circ \\ 0 & , \text{otherwise} \end{cases} \quad (15)$$

The factor inside the absolute value sign in equation (15) is a diffraction pattern dependent on the length of the diplane and the direction cosine on the seam axis OA. To understand how this diffraction pattern arises, it is sufficient to note that the diplane may be divided into a large number of strips parallel to the OA axis, each strip contributing to the diffraction pattern in equation (15). The second term represents the effective back-scattering area of the diplane for normal incidence on the seam axis OA. Taking note that

$$\sin\psi = \frac{\sin\phi}{(\cos^2\phi \sin^2\theta + \sin^2\phi)^{1/2}} \quad , \quad (16)$$

$$\begin{aligned} \sin(90-\psi) &= \cos\psi \\ &= \frac{\cos\phi \cos\theta}{(\cos^2\phi \sin^2\theta + \sin^2\phi)^{1/2}} \quad , \end{aligned} \quad (17)$$

and

$$\cos\phi \cos\theta, \sin\phi \geq 0 \text{ if, and only if } 0^\circ \leq \theta, \phi \leq 90^\circ \quad (18)$$

equation (15) may be rewritten as

$$\begin{aligned} A_e^{(2)}(\theta, \phi) \Big|_{OA} &= 2a^2 \left| \frac{\sin(2\pi a \cos\phi \cos\theta/\lambda)}{2\pi a \cos\phi \cos\theta/\lambda} \right| \cdot \left\{ \frac{\text{smaller of } |\cos\phi \sin\theta, \sin\phi|}{(\cos^2\phi \sin^2\theta + \sin^2\phi)^{1/2}} \right\} \\ &\cdot \frac{[1 + \text{sign}(\cos\phi \sin\theta)]}{2} \cdot \frac{[1 + \text{sign}(\sin\phi)]}{2} \end{aligned} \quad (19)$$

Figure 8 shows a plot of $A_e^{(2)}(\theta=90^\circ, \phi)/a^2$ as a function of ϕ , that is, when OS is perpendicular to the seam axis OA.

3.2.1 Effective Back-Scattering Area Due to Two Reflections From Cluster Surfaces

In the cluster of Figure 2, there are effectively eight diplanes of which two are associated with seam axis OA, two are associated with seam axis OB and four are associated with seam axis OC. Using the solution given

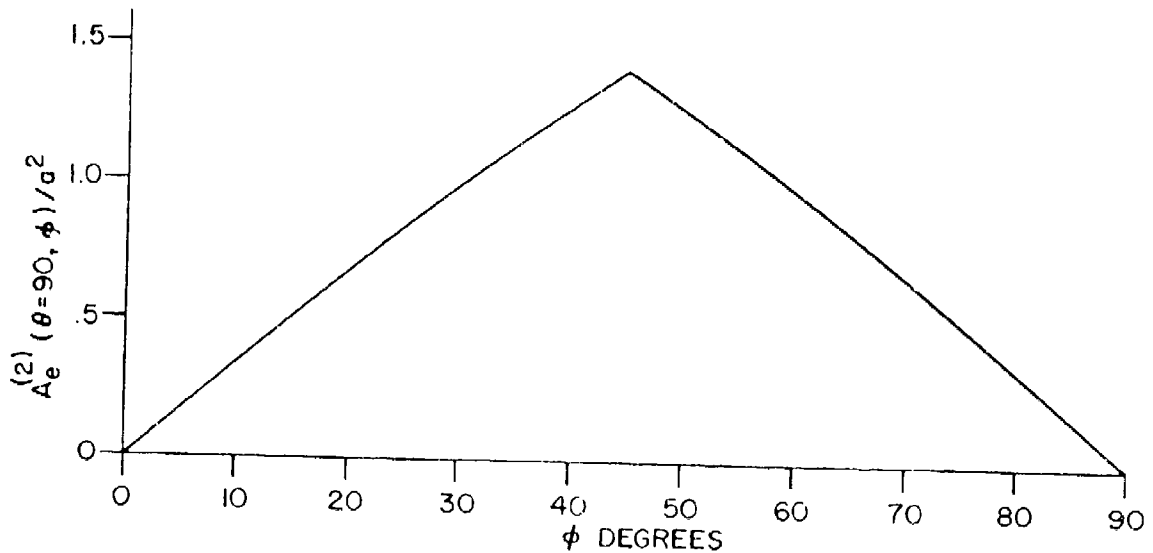


Figure 8. Plot of $A_e^{(2)}(\theta=90, \phi)/a^2$ as a function of ϕ

in equation (19) as a guide, the effective back-scattering area due to two reflections at the cluster surfaces may be written as

$$\begin{aligned}
 A_e^{(2)}(\theta, \phi) = & 4a^2 \left| \frac{\sin(4\pi a \cos \phi \cos \theta / \lambda)}{4\pi a \cos \phi \cos \theta / \lambda} \right| \cdot \left\{ \frac{\text{smaller of } [|\cos \phi \sin \theta|, \sin \phi]}{(\cos^2 \phi \sin^2 \theta + \sin^2 \phi)^{1/2}} \right\} \\
 & \cdot \frac{[1 + \text{sign}(\sin \phi)]}{2} \\
 + & 4a^2 \left| \frac{\sin(4\pi a \cos \phi \sin \theta / \lambda)}{4\pi a \cos \phi \sin \theta / \lambda} \right| \cdot \left\{ \frac{\text{smaller of } [|\cos \phi \cos \theta|, \sin \phi]}{(\cos^2 \phi \cos^2 \theta + \sin^2 \phi)^{1/2}} \right\} \\
 & \cdot \frac{[1 + \text{sign}(\sin \phi)]}{2} \\
 + & 2a^2 \left| \frac{\sin(2\pi a \sin \phi / \lambda)}{2\pi a \sin \phi / \lambda} \right| \cdot \left\{ \frac{\text{smaller of } [|\cos \phi \cos \theta|, |\cos \phi \sin \theta|]}{\cos \phi} \right\} \quad (20)
 \end{aligned}$$

The first term in equation (20) is the effective back-scattering area due to diplanes with seam axis OA. These diplanes have lengths $2a$ along the seam axis. Similarly, the second term is the effective back-scattering area due to diplanes with seam axis OB. The third term is the effective back-scattering area due to diplanes with seam axis OC. The function $[1 + \text{sign}(\sin \phi)]/2$ is included in equation (20), since we are interested only in back-scattering from the front of the cluster.

3.3 EFFECTIVE BACK-SCATTERING AREA DUE TO THREE REFLECTIONS

An expression for the effective back-scattering area due to three reflections from a corner reflector may be found in Reference [1]. In the present report, it shall be written as

$$A_e^{(3)}(\theta, \phi) = \begin{cases} 0, & \ell < 0 \\ 4a^2 \ell m/n, & \ell > 0, m \leq n/2 \\ a^2 \ell (4 - n/m), & \ell > 0, m > n/2 \end{cases} \quad (21)$$

where

$$\ell = \text{smallest of } [\cos\phi \cos\theta, \cos\phi \sin\theta, \sin\phi] \quad (22)$$

$$n = \text{largest of } [\cos\phi \cos\theta, \cos\phi \sin\theta, \sin\phi] \quad (23)$$

$$m = \text{remainder of } [\cos\phi \cos\theta, \cos\phi \sin\theta, \sin\phi] \quad (24)$$

$$\text{or } m = \cos\phi \cos\theta + \cos\phi \sin\theta + \sin\phi - \ell - n, \quad (25)$$

for $\cos\phi \sin\theta, \sin\phi \geq 0$ if, and only if $0^\circ \leq \theta, \phi \leq 90^\circ$.

It can be shown that the maximum value of $A_e^{(3)}(\theta, \phi)$ will occur when

$$\ell = m = n = 1/\sqrt{3} \quad (26)$$

resulting in a maximum value of the effective back-scattering area due to three reflections:

$$A_e^{(3)}(\theta, \phi) = a^2 \sqrt{3}. \quad (27)$$

The direction at which this maximum occurs may be determined from equations (22) - (24). The resulting values for θ and ϕ are 45.0° and 35.26° respectively. Figure 9 show plots of $A_e^{(3)}(\theta, \phi)/a^2$ as a function of θ for various values of ϕ . For fixed values of ϕ the effective back-scattering area due to three reflections reaches a maximum at $\theta = 45.0^\circ$. As stated earlier, this maximum is largest at $\phi = 35.26^\circ$.

3.3.1 Effective Back-Scattering Area Due to Three Reflections From Cluster Surfaces

Using the result for three reflections given in equations (21) - (25) as a guide, the effective back-scattering area due to three reflections from the cluster surfaces in Figure 2 may be given as

$$A_e^{(3)}(\theta, \phi) = \begin{cases} 0, & \ell < 0 \\ 4a^2 \ell m/n, & \ell > 0, m \leq n/2 \\ a^2 \ell (4 - n/m), & \ell > 0, m > n/2 \end{cases} \quad (28)$$

where

$$\ell = \text{smallest of } [|\cos\phi \cos\theta|, |\cos\phi \sin\theta|, \sin\phi] \quad (29)$$

$$n = \text{largest of } [|\cos\phi \cos\theta|, |\cos\phi \sin\theta|, \sin\phi] \quad (30)$$

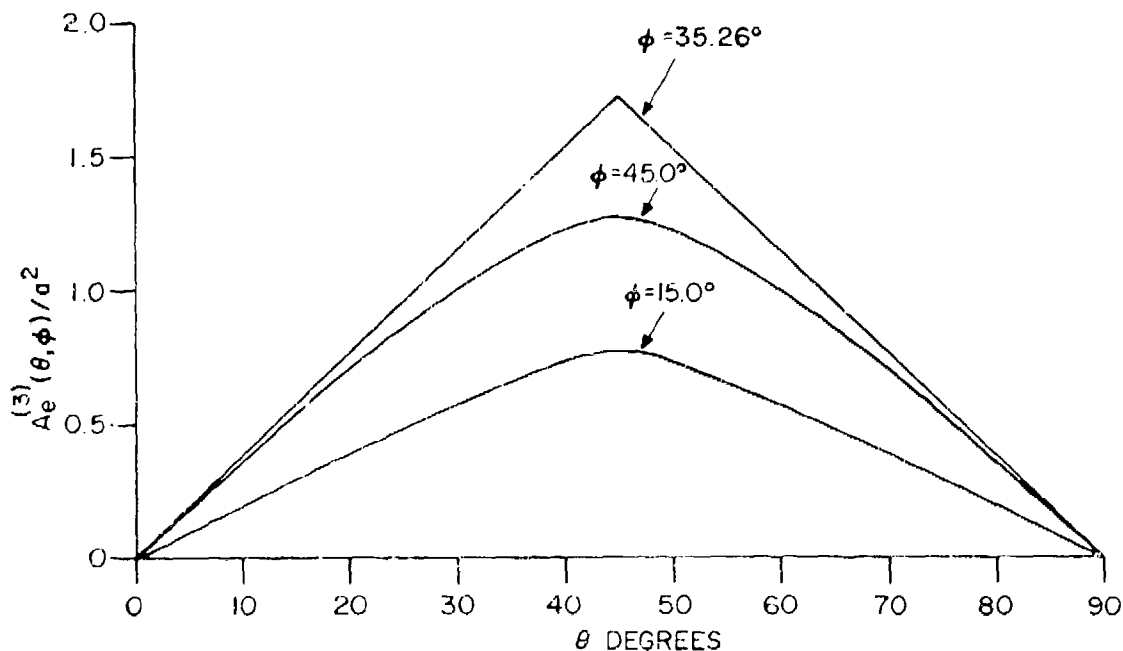


Figure 9. Plot of $A_e^{(3)}(\theta, \phi)/a^2$ as a function of θ for various values of ϕ

$$m = \text{remainder of } [|\cos\phi \cos\theta|, |\cos\phi \sin\theta|, \sin\phi] \quad (31)$$

for all values of θ and $\sin\phi \geq 0$ if, and only if $0^\circ \leq \phi \leq 180^\circ$.

4. DETERMINATION OF THE RADAR CROSS-SECTION FOR A CLUSTER OF CORNER REFLECTORS

In equation (3), the radar cross-section is given in terms of θ and ϕ as

$$\sigma(\theta, \phi) = \frac{4\pi [A_e(\theta, \phi)]^2}{\lambda^2} \quad (32)$$

where

$$A_e(\theta, \phi) = A_e^{(1)}(\theta, \phi) + A_e^{(2)}(\theta, \phi) + A_e^{(3)}(\theta, \phi). \quad (33)$$

Parameter $\sigma(\theta, \phi)$, which has the dimensions of area, may be expressed in decibels relative to a one square-metre target as

$$\sigma(\theta, \phi) \text{ dB}_{SM} = 10 \log_{10} [(\sigma(\theta, \phi)/1M^2)] \quad (34)$$

provided $A_e(\theta, \phi)$ and λ^2 are expressed in square metres.

In the results to be presented in Section 5, plots are made of the radar cross-section in decibels relative to a one square-metre target according to equation (34) for the cluster illustrated in Figure 2. Since this cluster of four corner reflectors is symmetrical about axes OA and OB, one can verify that

$$\begin{aligned}\sigma(\theta, \phi) &= (\theta + 0, \phi) \\ &= (\theta - 0, \phi) .\end{aligned}\tag{35}$$

Thus, we need only plot $\sigma(\theta, \phi)$ for $0^\circ \leq \theta \leq 45^\circ$ since beyond this range $\sigma(\theta, \phi)$ repeats.

5. DISCUSSION OF RESULTS FOR A CLUSTER OF FOUR SQUARE-CORNER REFLECTORS

In the following results, plots are made of the radar cross-section in decibels relative to a one square-metre target against θ for various values of ϕ , with $a = 0.225$ metres and $\lambda = 0.030$ metres. This choice for a is based on the cluster which is to be used by DRES. In addition, plots are made of the normalized effective back-scattering areas due to single, double and triple reflections which give rise to the plots of the radar cross-section. Since the relative phases of the multiple reflections at the corner surfaces have been ignored, the result for the radar cross-section is the same as the average of many measurements in the neighbourhood of (θ, ϕ) .

Figure 10 shows a plot of the radar cross-section in decibels as a function of θ for a value of $\phi = 35.26^\circ$ for the cluster of four square-corner reflectors in Figure 2. Figure 11 show plots of the individual effective back-scattering areas which gave rise to the total radar cross section in Figure 10. It may be noted that the major contribution to the total radar cross-section when $\theta = 0.0^\circ$ is through two reflections; the contribution due to one reflection being insignificant. However, as θ increases, the resultant effective back-scattering area due to two reflections decreases but that due to three reflections increases and peaks at $\theta = 45.0^\circ$. At this value of θ , the resultant effective back-scattering area is due almost entirely to three reflections.

Figure 12 shows a plot of $\sigma(\theta, \phi)$ dBsm against θ for a value of $\phi = 0.0^\circ$. Figure 13 show plots of the individual effective areas which gave rise to the results in Figure 12. It may be noted that when $\theta = 0.0^\circ$, the effective back-scattering area is due to one reflection from the cluster surface on the OAC plane. However, as θ increases, the effective back-scattering area due to one reflection decreases but that due to two reflections increases and peaks at $\theta = 45.0^\circ$. At this value of θ , the resultant effective area is due almost entirely to two reflections from the diplane with seam axis OC.

In Figure 14, where the direction of the radar is perpendicular to the surface of the cluster on the OAB plane, $\sigma(\theta, \phi=90)$ remains constant for all values of θ . This result is to have been expected since in this direction, a square, flat surface is observed which has four times the area of any one surface of a single corner reflector, in turn reflecting a constant amount of energy through one reflection for all values of θ . The effective back-

scattering area due to one reflection which gave rise to the result in Figure 14 is illustrated in Figure 15.

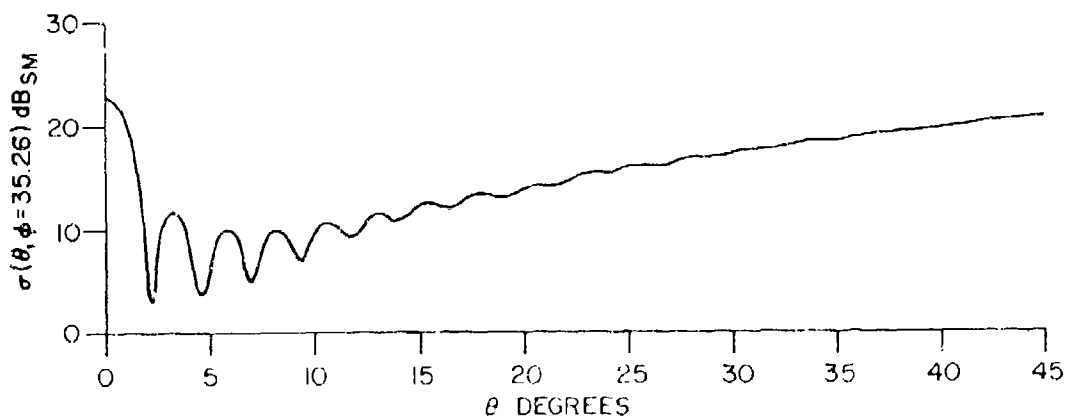


Figure 10. Plot of $\sigma(\theta, \phi = 35.26)$ dB_{SM} as a function of θ for a cluster of four square-corner reflectors
a = 0.225 metres, λ = 0.030 metres (X-Band).

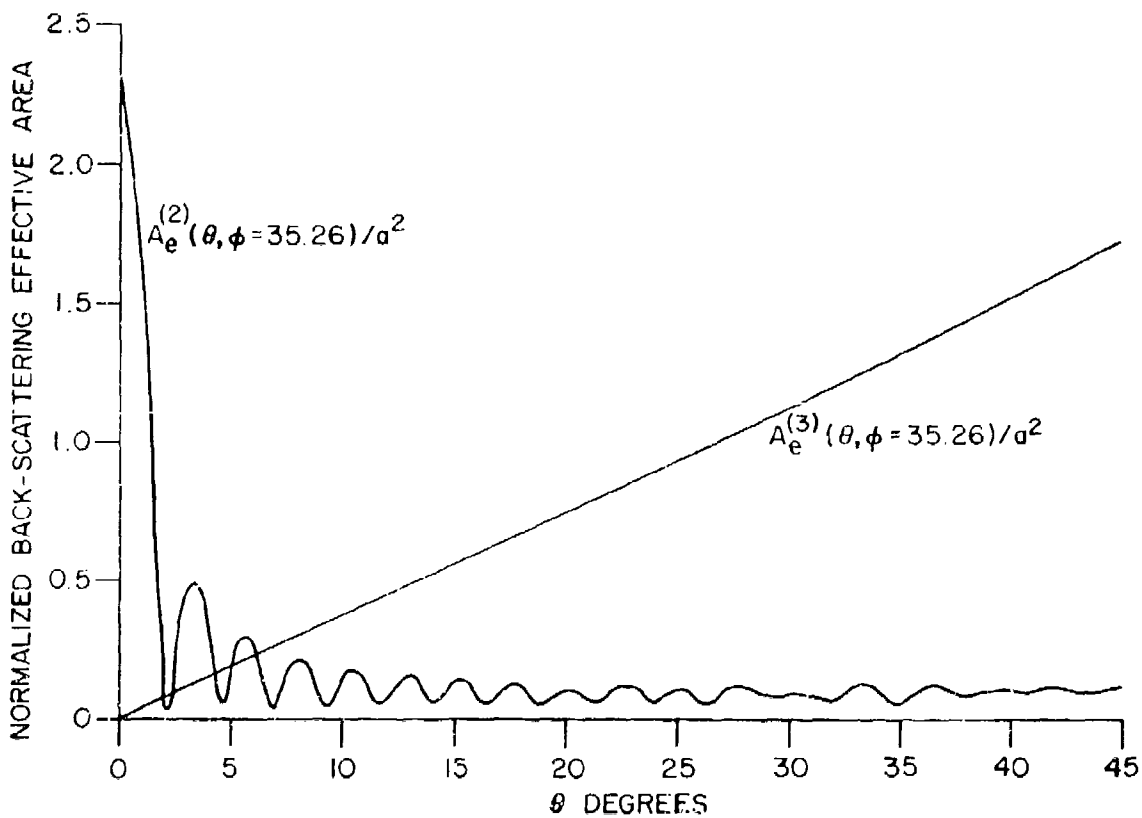


Figure 11. Plot of $A_e^{(2)}(\theta, \phi = 35.26)/a^2$ and $A_e^{(3)}(\theta, \phi = 35.26)/a^2$ as a function of θ

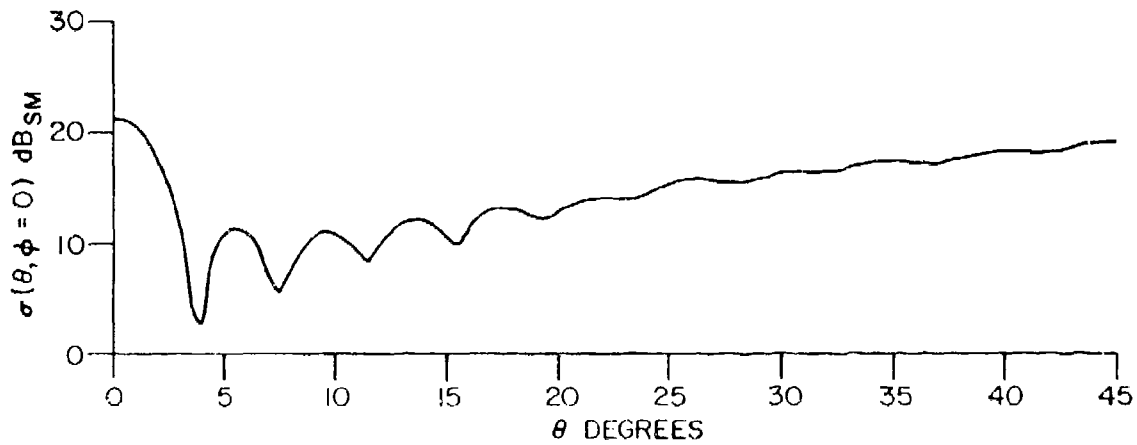


Figure 12. Plot of $\sigma(\theta, \phi=0)$ dB_{SM} as a function of θ for a cluster of four square-corner reflectors, $a=0.225$ metres, $\lambda=0.030$ metres (X-Band).

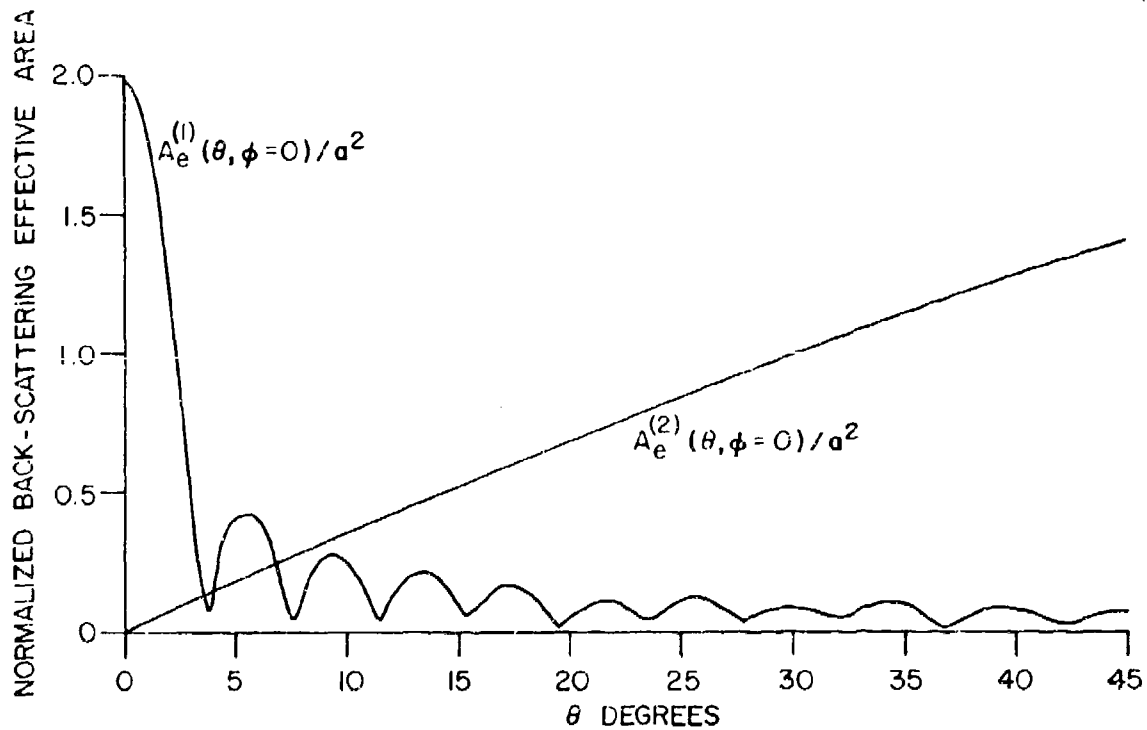


Figure 13. Plot of $A_e^{(1)}(\theta, \phi=0)/a^2$ and $A_e^{(2)}(\theta, \phi=0)/a^2$ as a function of θ

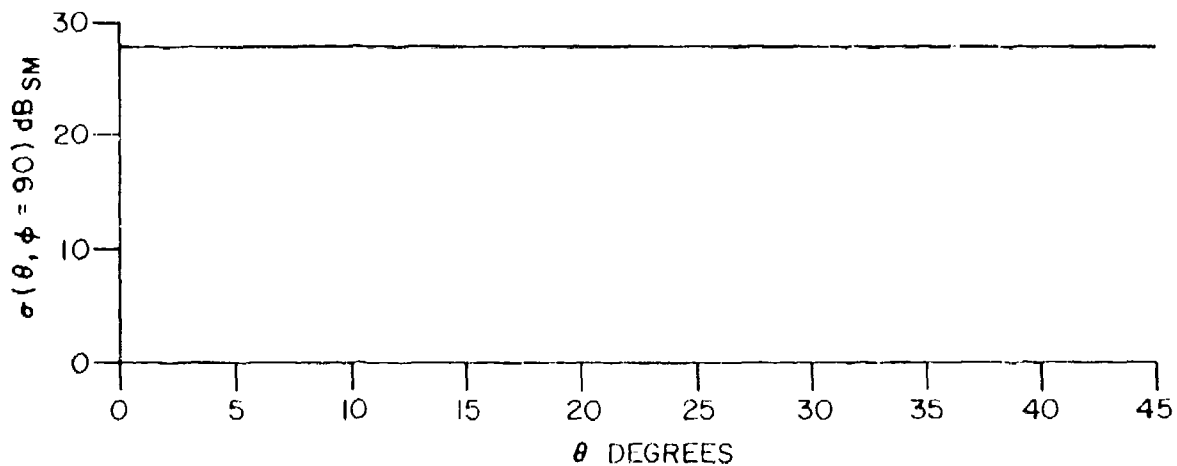


Figure 14. Plot of $\sigma(\theta, \phi = 90)$ dB_{SM} as a function of θ for a cluster of four square corner reflectors, $a = 0.225$ metres, $\lambda = 0.030$ metres (X-Band).

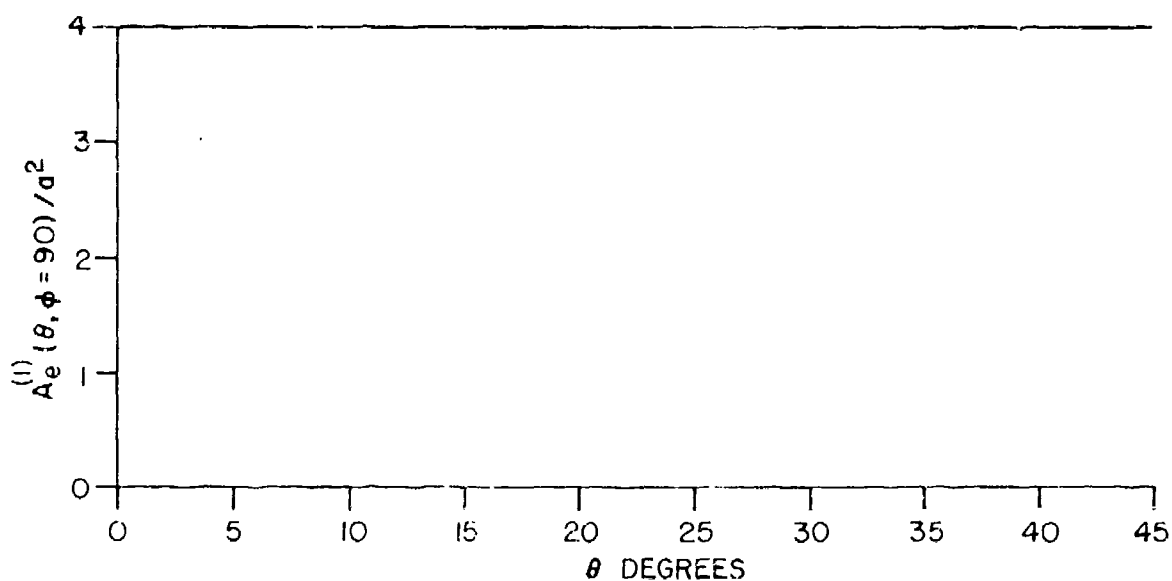


Figure 15. Plot of $A_e^{(1)}(\theta, \phi = 90) / a^2$ as a function of θ

As a further example of the way in which electromagnetic energy is back-scattered from this cluster, Figure 16 shows a plot of the radar cross-section in decibels relative to a one square-metre target against ϕ at $\theta = 45.0^\circ$. Figure 17 show plots of individual back-scattering areas due to single, double and triple reflections which gave rise to the results in Figure 16. When $\phi = 0.0^\circ$, the resultant effective area is due to two reflections from the diplane surface with seam axis OC. However, as ϕ increases, the effective area due to two reflections decreases because of the

diffraction effect but the effective area due to three reflections increases reaching a peak at $\phi = 35.26^\circ$. As ϕ continues to increase, the effective area due to three reflections decreases, reducing to zero when $\phi = 90.0^\circ$. At this value of ϕ , the resultant effective area is due to one reflection from the surface of the cluster on the OAB plane. These results are instructive in that they illustrate the dependence on ϕ of effective back-scattering areas due to single, double and triple reflections.

5.1 DISCUSSION OF RESULTS OF THE AVERAGE RADAR CROSS-SECTION FOR A CLUSTER OF FOUR SQUARE-CORNER REFLECTORS

Generally, the average radar cross-section is a useful measure of the ability of the cluster to reflect electromagnetic energy back to the source. Figure 18 shows a plot of the average radar cross-section $\sigma_{AV}(\phi)$ in decibels relative to a one square-metre target (averaged over one revolution in θ) against ϕ . It may be noted from these results that this cluster has an average radar cross-section which exceeds that of a one square-metre target over the entire range of ϕ . When $\phi = 0.0^\circ$, the average radar cross-section is due to one reflection from the surfaces on the OAC and OBC planes and from two reflections from diplanes with seam axis OC. When $\phi = 90.0^\circ$, the resultant average radar cross-section is due to one reflection from the surface on the OAB plane. In the remaining portion of the plot, the resultant average radar cross-section is due to a combination of single, double and triple reflections.

6. CALCULATION OF THE AVERAGE RADAR CROSS-SECTION FOR THE CLUSTER ILLUSTRATED IN FIGURE 1

In Figure 19, a cluster of corner reflectors of the type illustrated in Figure 1 is superimposed on a cluster of four square-corner reflectors. When the direction of the radar is perpendicular to the OAC plane (i.e., $\phi = 0.0^\circ$), the physical areas of both clusters are identical; therefore, the average radar cross-section for both clusters will be identical. When the direction of the radar is perpendicular to the OAB plane (i.e., $\phi = 90.0^\circ$), a circular plate and a square plate are observed. The physical area of the circular plate is smaller than that of square plate by a factor of $\pi/4$. Consequently, the average radar cross-section due to the circular plate will be smaller than that due to the square plate by this factor.

Let the average radar cross section $\sigma_{CIRC}(\phi)$ for the cluster illustrated in Figure 1 be given in terms of the average radar cross-section $\sigma_{AV}(\phi)$ for the cluster illustrated in Figure 2 as

$$\sigma_{CIRC}(\phi) = K(\phi) \sigma_{AV}(\phi) \quad (36)$$

We know that

$$K(\phi) = 1 \text{ for } \phi = 0.0^\circ, \quad (37)$$

and

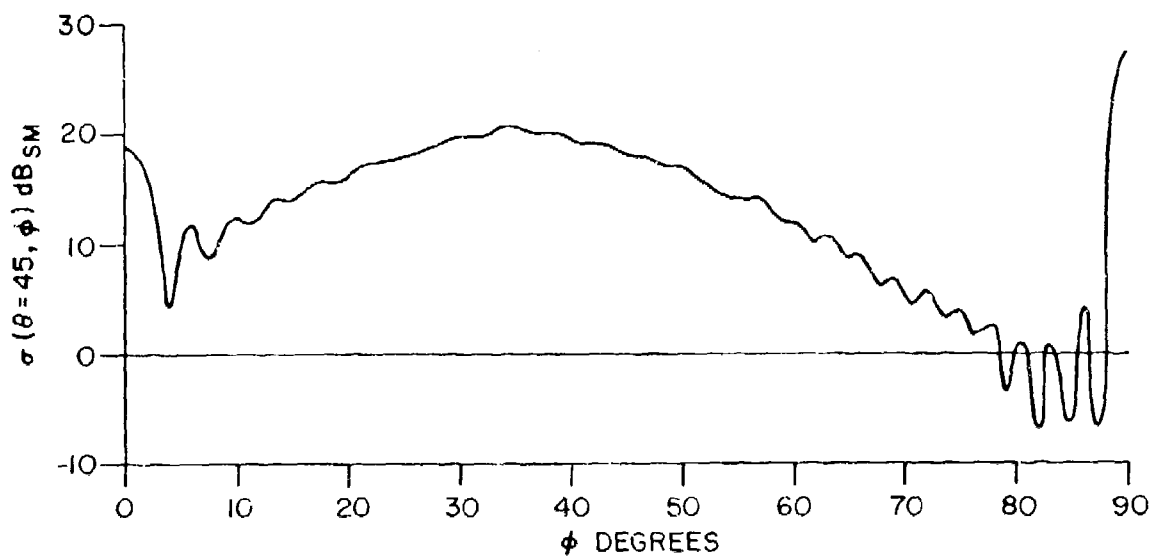


Figure 16. Plot of $\sigma(\theta=45, \phi)$ dB_{SM} as a function of ϕ for a cluster of four square-corner reflectors
 $a = 0.225$ metres, $\lambda = 0.030$ metres (X-Band).

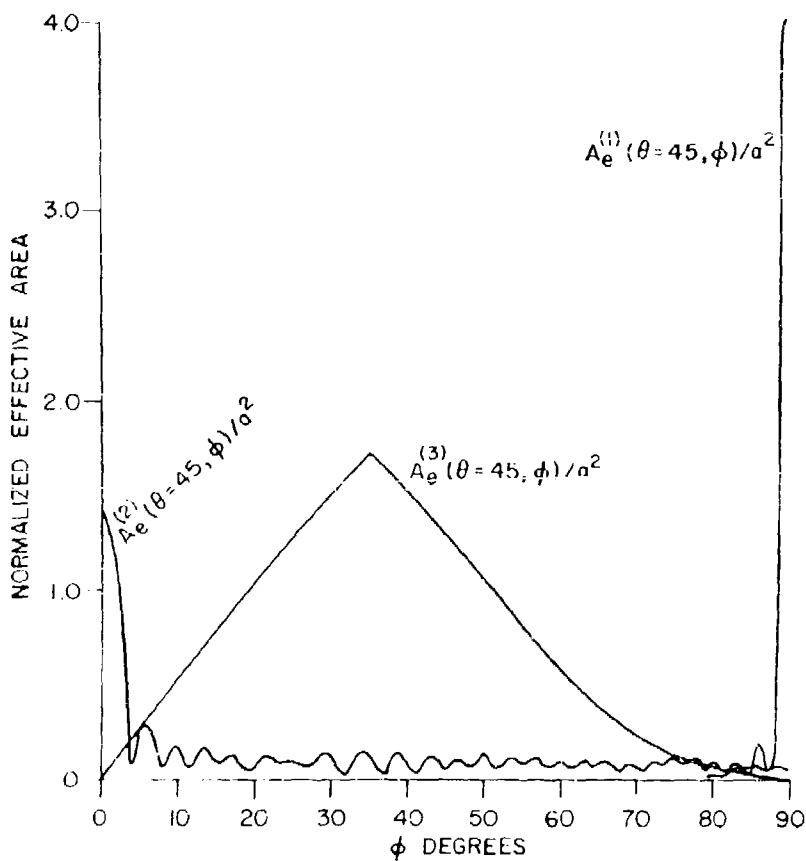


Figure 17. Plot of $A_e^{(1)}(\theta=45, \phi)/a^2$, $A_e^{(2)}(\theta=45, \phi)/a^2$ and $A_e^{(3)}(\theta=45, \phi)/a^2$ as a function of ϕ .

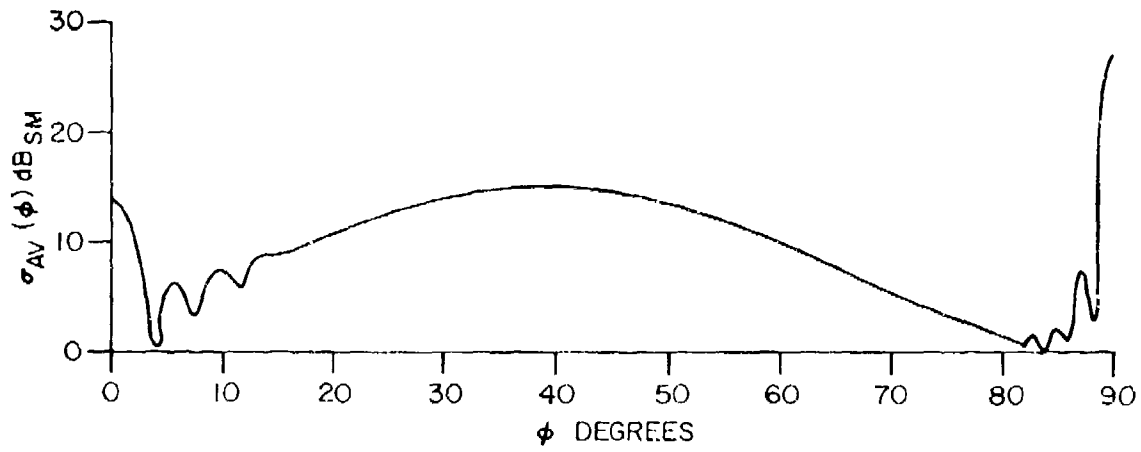


Figure 18. Plot of $\sigma_{AV}(\phi)$ as a function of ϕ for a cluster of four square-corner reflectors, $a = 0.225$ metres, $\lambda = 0.030$ metres (X-Band)

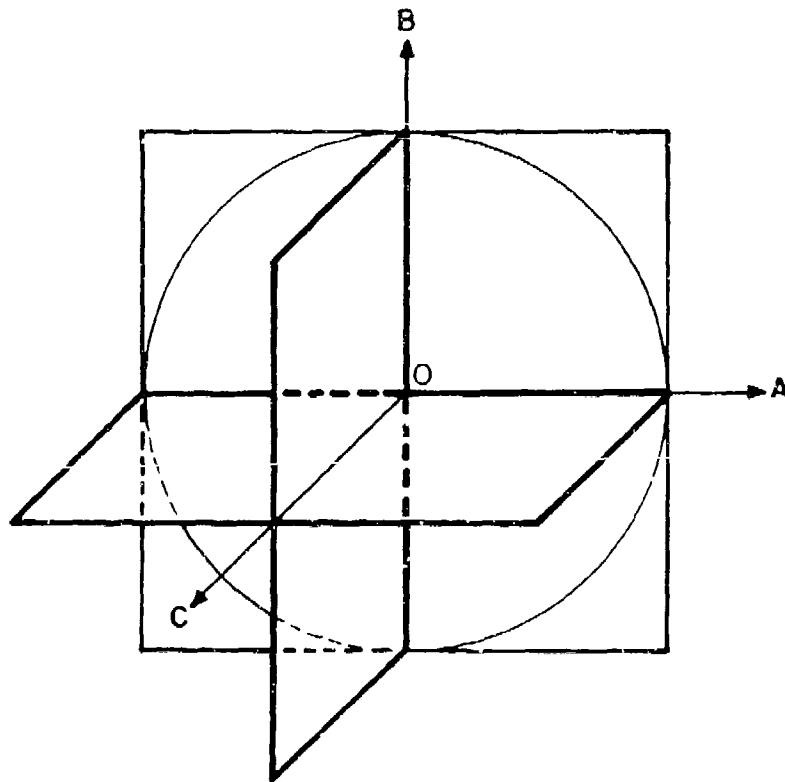


Figure 19. Diagram of the cluster illustrated in Figure 1 superimposed on a cluster of four square-corner reflectors.

$$K(\phi) = (\pi/4)^2 \text{ for } \phi = 90.0^\circ \quad (38)$$

For other values of ϕ , $K(\phi)$ is not known. We now make the assumption that $K(\phi)$ decreases linearly from unity to $(\pi/4)^2$ as ϕ changes from 0.0° to 90.0° , that is,

$$K(\phi) = 1 + \frac{\phi}{90} (\pi^2/16 - 1). \quad (39)$$

With this expression for $K(\phi)$, average values of radar cross-section may be determined for the cluster of corner reflectors illustrated in Figure 1 from average values of radar cross-section for the cluster of square-corner reflectors illustrated in Figure 2. A plot of $K(\phi)$ in decibels against ϕ is shown in Figure 20.

Figure 21 shows a plot of the average radar cross section $\sigma_{\text{CIRC}}(\phi)$ in decibels relative to a one square-metre target for the cluster illustrated in Figure 1 from values of $\sigma_{\text{AV}}(\phi)$ for the cluster illustrated in Figure 2 according to equation (36). It may be noted that this cluster has an average radar cross-section which exceeds that of a one square-metre target over a very large portion of the range of angles in ϕ .

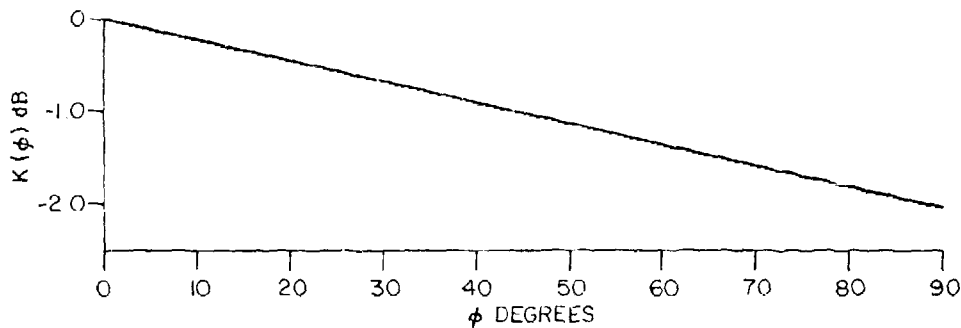


Figure 20. Plot of $K(\phi)$ in decibels as a function of ϕ

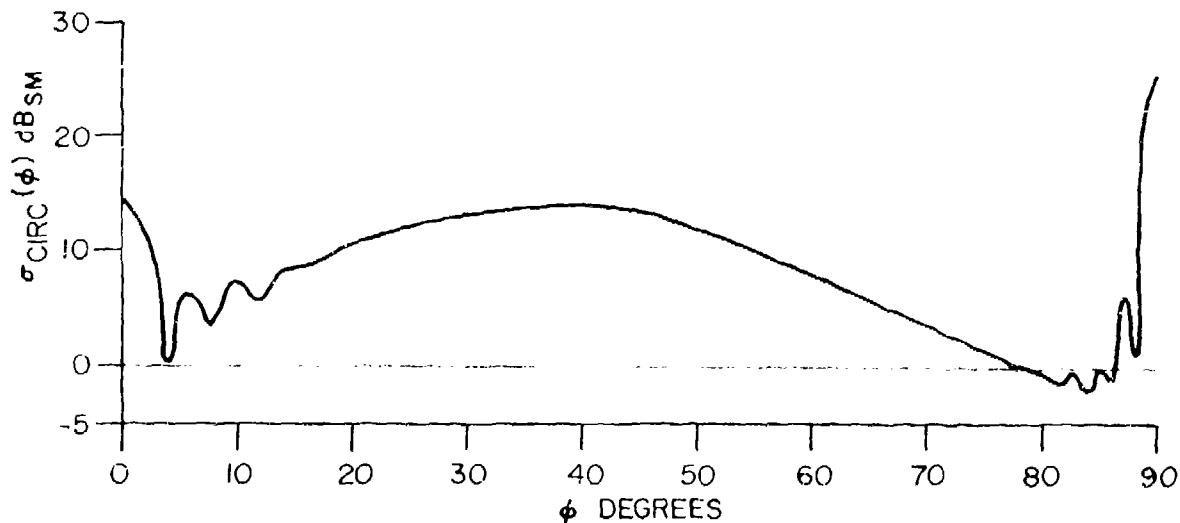


Figure 21. Plot of $\sigma_{\text{CIRC}}(\phi)$ dB SM as a function of ϕ for the cluster of Figure 1, $a = 0.225$ metres, $\lambda = 0.030$ metres (X-Band).

7. SUMMARY AND CONCLUSIONS

It has been shown that the resultant effective back-scattering area of a cluster of four square-corner reflectors may be decomposed into the effective back-scattering areas due to single, double and triple reflections. From the computation of the effective area of this cluster, approximate values of the average radar cross-section have been determined for the cluster of corner reflectors with a circular back-plate. These results show that, for corner reflectors having sides of 0.225m length, the radar cross-section exceeds that of a one square-metre target over a wide range of incident angles at X-Band frequencies. The results presented in this report apply to the case where free-space propagation prevails and therefore do not include the effects of multipath and other transmission anomalies which arise in practice.

8. ACKNOWLEDGEMENTS

Useful discussions with Dr. E.K.L. Hung are acknowledged. This work is supported by the Department of National Defence, Ottawa, Canada.

9. REFERENCES

1. Spencer, R.C., *Optical Theory of the Corner Reflector*, M.I.T. Radiation Laboratory, Report 433, March 1944.
2. Robertson, Sloan D., *Targets for Microwave Radar Navigation*, Bell System Tech. J., Vol. 26, pp. 852 - 869, October 1947.
3. Steinberg, Bernard D., *Principles of Aperture and Array System Design*, John Wiley and Sons, 1976, p. 6.
4. Skolnik, M.I., *Radar Handbook*, McGraw-Hill Book Company, 1970, p. 9-12.
5. Barton, David K., *Radar Systems Analysis*, Prentice-Hall, 1964, Chapter 4.